Atmospheric Pollution Research 12 (2021) 101086

Contents lists available at ScienceDirect

Atmospheric Pollution Research

journal homepage: www.elsevier.com/locate/apr

Cluster analysis of atmospheric particle number size distributions at a rural site downwind of Seoul, Korea

Yonghwan Lee [a], Yongjoo Choi [a,b], Hyungjun An [a], Jisoo Park [a], Young Sung Ghim [a,*]

[a] Department of Environmental Science, Hankuk University of Foreign Studies, Yongin, Gyeonggi, 17035, South Korea
[b] Now at Research Institute for Global Change, Japan Agency for Marine-Earth Science and Technology (JAMSTEC), Yokohama, 236-0001, Japan

ARTICLE INFO

Keywords:
k-means clustering
Cluster separation
Characterization and identification
Traffic emissions
New particle formation

ABSTRACT

We identified seven clusters from SMPS measurements ranging from 10 to 291 nm using k-means clustering, representing background (BG), local emissions (LocEm), two types of traffic emissions (TR), and three types of nucleation (NC). BG and LocEm differed in that pollutant concentrations were low and high, respectively, but both exhibited less pronounced diurnal variations in the frequency of occurrence. TR was divided into larger particles peaking at 72 nm and smaller particles with a primary peak at ~10 nm and a secondary peak at 72 nm. Because the main road is more than 1 km away from the study site, the primary peak consisting of smaller particles in the nucleation mode disappeared in most cases. However, when being affected directly from vehicle emissions, the primary peak size was reduced by the volatilization of semi-volatile substances. NC was divided into NC (fresh), NC (aged), and NC (trans) denoting nucleated far away and transported. NC (fresh) had a peak size of 21 nm and a peak time of 13:00, along with typical conditions favorable for new particle formation (NPF). The highest ozone and lowest PM_{10} concentrations for NC (aged) were conducive to particle growth, because semi-volatile substances were actively produced, while the condensation sink of these substances onto pre-existing particles was unavailable. Many characteristics of NC (trans) were similar to BG and LocEm, indicating NPF over a wider area. Because of the distance to the main road, the contribution to the nucleation mode was 44% for NC, higher than 26% for TR.

1. Introduction

The public's concern about particulate matter (PM) is high over the world. In most countries, PM is regulated of mass concentration. PM policies for two size ranges, such as PM_{10} (PM with an aerodynamic diameter $\leq$ 10 μm) and $PM_{2.5}$ (PM with an aerodynamic diameter $\leq$ 2.5 μm), are plausible, in that measurement methods are simpler and clearer than are other metrics based on physical and chemical properties. However, there are still many uncertainties about which properties of PM are a health risk (World Health Organization, 2003, 2013; NARSTO, 2004). Whereas PM mass is dominated by coarse (particle diameter ranged from ~1 μm to 10 μm) and fine (<~1 μm) particles, the number is dominated by ultrafine particles (<100 nm) in the nucleation (<~25 nm) and Aitken (~25–100 nm) modes. Ultrafine particle studies using the number concentration have a merit of tracing particle emissions and formation from the origin (Kulmala et al., 2014; Vu et al., 2015; Paasonen et al., 2016; Kerminen et al., 2018; Lee et al., 2019). The health effects of ultrafine particles known so far is mainly due to the physical nature of being small in size. Because these particles are small, they can penetrate deep into the alveoli, cause inflammation, and spread toxic substances to distant organs through the lung vasculature (HEI Review Panel on Ultrafine Particles, 2003; Schraufnagel, 2020). For the global environment, ultrafine particles are important because they can produce cloud condensation nuclei (CCN, > ~100 nm). When the CCN concentrations increase because there are many ultrafine particles, the cloud droplet size decreases, which leads to an increase in cloud albedo and a suppression of precipitation. As a consequence, the effects of clouds that contribute to cooling persist for a long time (Seinfeld and Pandis, 2006; Foster et al., 2007).

Ultrafine particles are mainly emitted from vehicles in urban areas, but are also emitted from other combustion sources such as biomass burning, incineration, and power plants (Kulmala et al., 2011; Vu et al., 2015; Paasonen et al., 2016; Kerminen et al., 2018). Whereas the number size distribution that results from the nucleation in the air is

Peer review under responsibility of Turkish National Committee for Air Pollution Research and Control.
* Corresponding author.
E-mail address: ysghim@hufs.ac.kr (Y.S. Ghim).

https://doi.org/10.1016/j.apr.2021.101086
Received 21 November 2020; Received in revised form 10 May 2021; Accepted 10 May 2021
Available online 13 May 2021

skewed toward sizes of a few nm or less (Seinfeld and Pandis, 2006; Kontkanen et al., 2017; Brilke et al., 2020), those from combustion sources depend on fuel and combustion conditions. Therefore, we can trace the possible origin of particles by examining their size distributions, and can also obtain information on the atmospheric processing of particles during transport from the origin, which alter the size distribution (Dall'Osto et al., 2011a, 2013; Brines et al., 2014, 2015).

Table 1 shows selected studies that attempted to estimate the origins by identifying the size distribution patterns. All the studies used cluster analysis, and the number of clusters ranged from 5 to 12. However, as in other studies for source identification and apportionment from the number size distribution, various receptor techniques including positive matrix factorization (PMF) have been attempted (Vu et al., 2015). In this study, we want to figure out all important sources that may be involved and their characteristics, rather than source apportionment, which left as a subject of a future study.

The origins are largely divided into four groups: background (or regional), local emissions, traffic, and nucleation (or photochemical). Whereas nucleation and background represent clusters with small and large particles, respectively, traffic and local emissions represent relatively small and large particles, respectively, whose peak sizes become smaller or larger depending on the emission sources. The lower limit of the size range is ~10 nm in roughly half the studies and ~3 nm in the other half. Despite the difference in the lower limit, both cluster separation and peak sizes are similar. In addition to the studies shown in Table 1, Sabaliauskas et al. (2013) classified eight clusters for traffic using measurement data on the roadside, ranging from 14 to 81 nm in peak size according to season and time of day. Wang et al. (2013) and Qi et al. (2015) classified five clusters, ranging from 40 to 200 nm and 60–110 nm in peak size, respectively, according to the direction of backward trajectories.

In this study, we measured the particle number size distribution at the rooftop of a five-story building on a hill, located downwind of Seoul, Korea (37.34 °N, 127.27 °E, 167 m above sea level; Fig. 1), using a scanning mobility particle sizer (SMPS). The study period was February 2015 to June 2016, except for July to September 2015 during which measurements were not made, because of inspection and maintenance of the SMPS. We also employed the clustering method to classify the size distribution patterns. We determined the number of clusters by reviewing the separation of clusters by increasing the number of clusters based on the validation statistics analysis. We characterized the clusters by examining the size distribution, diurnal and seasonal variations in the frequency of occurrence, meteorological parameters, and pollutant concentrations.

2. Methods

2.1. Study site

The study site is about 35 km southeast of the center of Seoul, downwind of the metropolitan area in the prevailing westerlies (Fig. 1). The site is located in a horseshoe-shaped forested valley with westward-facing slopes, over which biogenic emissions likely prevail. To the west is a rural area with small buildings, farmlands, and open spaces scattered on the sides of a 4-lane road and a river. A forest on the mountainside is adjacent to the north, and the bus depot is about 150 m downward to the south.

2.2. Measurements and data use

An SMPS consists of a differential mobility analyzer (Grimm Model 55-U) and condensation particle counter (Grimm Model 5.410). We measured the size distribution in the range from 5.1 to 290.8 nm with 86 channels at 10-min intervals in 2015, and in the range from 7.9 to 299.6 nm with 102 channels at 5-min intervals in 2016. We measured black carbon (BC) using Multi-Angle Absorption Photometer (MAAP 5012, Thermo Scientific) at 10-min intervals. To convert the absorption coefficient to mass concentration, we used 10.3 m^2/g for mass absorption efficiency, obtained from the intercomparison study between MAAP and a continuous soot monitoring system (COSMOS) (Kanaya et al., 2013), instead of the default value of 6.6 m^2/g. We measured wind speed and direction by a wind monitor (R. M. Young Model 05103), and measured air temperature and relative humidity (RH) by a temperature and humidity sensor (Useem UE-H100) at 10-min intervals.

We obtained hourly concentrations of criteria pollutants for which ambient air quality standards are established, such as SO_2, NO_2, CO, O_3 and PM_{10} from the nearest air pollution monitoring station (37.41 °N, 127.26 °E; Fig. 1), about 8 km north of the study site. We obtained hourly solar radiation from the Seoul Metropolitan Office of Meteorology (37.27° N, 126.99° E, 34.1 m asl; Fig. 1), about 26 km west-southwest of the study site.

Table 1
Selected studies for characterizing the number size distributions by clustering method.

Reference	Study site (period)	Size range (nm)	Number of clusters	Clusters[a] (peak size, nm)[b]
This study	Rural, Seoul Metropolitan Area, Korea (Feb. 2015–Jun. 2016)	10–291	7	Background (80); Local emissions (84); Traffic - larger particles (72), smaller particles (10, 72); Nucleation - fresh (21), aged (38), transported (30)
Dall'Osto et al. (2011b)	Remote, Mace Head, Ireland (Jan. 1 – Nov. 18, 2008)	3–500	12	Coastal nucleation 1 (4.5), 2 (6.5), 3 (10.2); Open-ocean nucleation and growth 1 (15), 2 (28), 3 (40); Anthropogenic 1 (42), 2 (62), 3 (112); Background clean marine 1 (30, 165), 2 (52, 212), 3 (112, 372)
Dall'Osto et al. (2012)	Urban background, Barcelona, Spain (2004)	13–800	9	Local pollution diluted by strong wind 1 (26), 2 (21); Traffic 1 (22), 2 (41), 3 (29); Photochemical 1 (18), 2 (80); Background 1 (90), 2 (55)
Wegner et al. (2012)	Semi-urban, Helsinki, Finland (2006–2008)	3–950	7	Traffic (19, 71); Aged maritime (102); Nucleation (5); District heating/wood combustion, traffic (afternoon rush-hour) (16); Nocturnal (49); Traffic, district heating (morning rush-hour) (24); Maritime origin (69)
Ripamonti et al. (2013)	Semi-urban, Helsinki, Finland (Jan. 2008–Dec. 2010)	3–950	6	Local anthropogenic (traffic, domestic and district heating) 1 (~12), 2 (~19); Aged (~40); Maritime origin 1 (~55), 2 (~90); Traffic and local (~15, ~65)
Brines et al. (2014)	4 sites, Barcelona, Spain (Sep. 20 - Oct. 20, 2010)	11-322, 15–228, 10-470	9	Traffic 1 (23), 2 (24), 3 (15, 42); Urban background 1 (16, 53); Regional background 1 (135), 2 (77); Nucleation (15); Regional nitrate (52); Mix (39)
Salimi et al. (2014)	25 sites, Brisbane, Australia (Oct. 2010–Aug. 2012)	9–414	5	Nucleation - fresh (<9), aged (<20); Traffic (20); Background - biomass burning (60), background (40)
Agudelo- Castañeda et al. (2019)	Urban, Porto Alegre, Brazil (Jan.–Sep., 2015)	2.5–250	8	Traffic - fresh (20), aged (20–30); Background - nocturnal (90), biomass burning (50–60), background (20, 70); Nucleation - fresh (<5), regional (~15), growth (<20)

[a] Main categories are divided by semicolons as necessary.
[b] Primary peak unless the secondary and tertiary peaks are noticeable. Some values are taken from the figure.

2.3. Data processing

Considering different size ranges and channels of SMPS measurements in 2015 and 2016, we prepared hourly data for the size distribution ranging from 10.3 to 290.8 nm with 70 channels, using an R function for a cubic spline interpolation (https://www.rdocumentation.org/packages/stats/versions/3.6.2/topics/smooth.spline). Total amount of hourly data was 7054; by season, there were 3,758, 954, 840, and 1502 in spring, summer, fall, and winter, respectively. Compared to the possible amount of data from the full operation of SMPS, they correspond to 85%, 38%, 38%, and 55%, respectively, for each season, and 60% for the total. The percentages for summer and fall are low at 38% because SMPS measurement was not made from July to September 2015, whereas that for spring is high at 85% because most SMPS measurements proceeded smoothly in both 2015 and 2016.

We employed the clustering method to identify the size distribution patterns. Although various clustering methods had been tested since Beddows et al. (2009), all the studies shown in Table 1 used k-means clustering. The number of clusters was generally determined by checking the cluster validation statistics, such as the Dunn index and silhouette width. However, since this procedure is solely statistical, it is common to determine the number of clusters by reviewing the characteristics of the clusters (including the size distribution) as well (Dall'Osto et al., 2012; Wegner et al., 2012; Brines et al., 2014; 2015; Salami et al., 2014). In this study, we classified the size distribution using an R function k-means (https://www.rdocumentation.org/packages/stats/versions/3.6.2/topics/kmeans). We examined the variations in the validation statistics with the number of clusters by calculating the Dunn index and silhouette width using cluster.stats (https://www.rdocumentation.org/packages/fpc/versions/1.1-1/topics/cluster.stats).

3. Results and discussion

3.1. Cluster validation statistics

Fig. 2 shows the variations in the Dunn index and silhouette width with the number of clusters. Since two and three clusters were too few for the size distribution patterns, we investigated the variations staring from 4 and up to 20, so that we could observe the variations with the number of clusters sufficiently. The Dunn index is the ratio of the minimum distance between two objects of different clusters to the maximum distance between two objects within a cluster (Wegner et al., 2012). Thus, the larger the Dunn index, the better the clusters are separated. The silhouette width measures the degree of confidence in the grouping of a particular object within the cluster, and has a value between −1 and 1 (Brock et al., 2008). The values near 1 indicate that the clusters are very dense and nicely separated, whereas negative values indicate that the objects may be placed in the wrong cluster. In Fig. 2, the silhouette width decreases with the number of clusters, except for 5–7 and 9 clusters, meaning that the reason for cluster separation reduces. On the other hand, the Dunn index is high at the numbers 15–17, except for the number 7, which is too large for classifying the size distributions.

3.2. Cluster separation and characterization

The characteristics of clusters were distinguished based on the size distribution, diurnal variation in the occurrence, pollutant concentrations, and meteorological parameters. For the characteristic values of the size distribution, the peak sizes and concentrations are presented in Fig. 3. At two clusters, relatively larger (LP) and smaller particles (SP) were separated. At three clusters, LP was divided into background (BG) and traffic clusters (TR), and SP was designated as nucleation (NC), because similar characteristics were maintained, as seen in the peak size

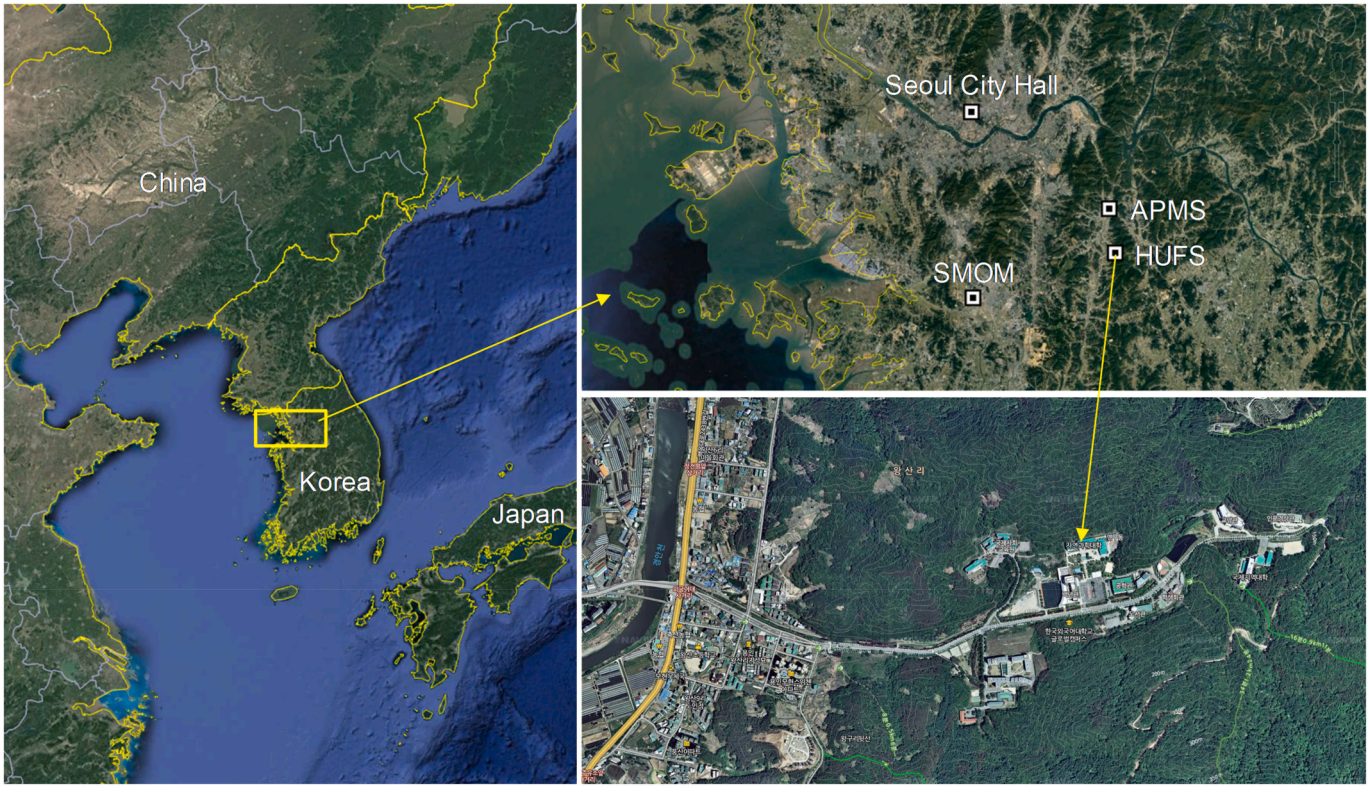

Fig. 1. Location of the study site in the Global Campus of Hankuk University of Foreign Studies (HUFS). The nearest air pollution monitoring station (APMS) operated by the National Institute of Environmental Research is about 8 km north, and the Seoul Metropolitan Office of Meteorology (SMOM) is about 26 km west-southwest, of the study site. The four-lane national road (shown in orange) along a river passes about 1.4 km to the west of the study site in the left-hand side of the lower-right panel.

and concentration. At four clusters, the cluster for local emissions (LocEm) was separated from BG, and for five clusters, NC was divided into NC (fresh) and NC (aged).

Fig. S1 shows the size distributions and diurnal variations in the frequency of occurrence for five clusters, and Table S1 summarizes selected pollutant concentrations and meteorological parameters. We also provide the number concentrations by mode in Table S1, which was defined by nucleation less than 25 nm, Aitken ranging from 25 to 100 nm, and accumulation greater than 100 nm. However, these values should be acknowledged with caution, because we considered only particles ranging from 10.3 to 290.8 nm, and excluded the nucleation and accumulation modes that fell on smaller and larger portions, respectively. In Table S1, BG exhibits the lowest number concentrations by mode and pollutant concentrations only higher than NC (aged) except O_3. LocEm has the second highest concentrations of CO, NO_2, and BC after TR, and above all, the lowest wind speed. The peak time at 2:00 can be attributed to low mixing height, which emphasized the effects of local emissions. The peak size of TR is smaller than those of BG and LocEm, but is larger than those of NCs because of the highest concentration of the accumulation mode. The concentrations of pollutants from vehicle emissions (such as CO, NO_2, and BC) are highest, and the peak times occur at 9:00 and 20:00, which are morning and evening rush hours, respectively. NC was classified into NC (fresh) and NC (aged); NC (fresh) has a small peak size of 13 nm, a peak time of 13:00, early afternoon, and the highest nucleation mode. The SO_2 concentration and solar radiation, which are key elements of new particle formation (NPF), are also highest. Compared to NC (fresh), NC (aged) has a larger peak size of 33 nm, a later peak time of 16:00, and the highest Aitken mode. The O_3 concentration is highest, whereas the concentrations of other pollutants are lowest.

NC (aged) was further divided into NC (aged) and NC (transported) (NC [trans]) at six clusters. Considering that the characteristics of the size distribution for six clusters are maintained mostly up to seven clusters, we examined the implication of this separation through Table 2 and Fig. S2 for seven clusters. However, we also prepared Fig. S4 and Table S2 in the Supplement to check the exact features of the six clusters as necessary. Whereas newly formed NC (aged) retains a significant portion of the original characteristics in peak size, peak time, and pollutant concentrations (Table 2), NC (trans) exhibits a high occurrence for a longer time from the beginning of NC (fresh) to the end of NC (aged) albeit at generally lower levels (Fig. S2(b)). As mentioned earlier, NC (fresh) for five clusters shows many aspects of NPF. However, PM_{10} concentration is highest, and the concentrations of CO, NO_2, and BC are lower than those for TR, but are comparable to those for LocEm. At seven clusters, TR (SP) was separated from NC (fresh). As TR (SP) was separated, NC (fresh) has the lowest concentrations of CO, NO_2, and BC, and O_3 concentration at the level of NC (aged). Solar radiation, temperature, and wind speed become the highest along with the lowest RH, which are typical meteorological conditions favorable for NPF (Vehkamäki et al., 2004; Hamed et al., 2007; Jeong et al., 2010; Kerminen et al., 2018). On the other hand, TR (SP) has the highest concentrations of most pollutants and the lowest O_3 concentration, only with NO_2 concentration lower than TR (LP). The size distribution of NC (fresh) changes significantly with the separation of TR (SP) (Fig. S3(a)). The peak size increases to 21 nm, and the secondary peak around 70 nm moves to TR (SP). The size distribution of TR (SP) consists of the primary peak of 10 nm and the secondary peak of 72 nm, which is the same as the peak size of TR (LP). Compared to TR (LP) whose occurrence peaks in the morning and evening rush hours, the occurrence of TR (SP) is high during the daytime, and O_3 concentration is low because of the titration of directly emitted NO (Ghim and Chang, 2000; Fujita et al., 2003).

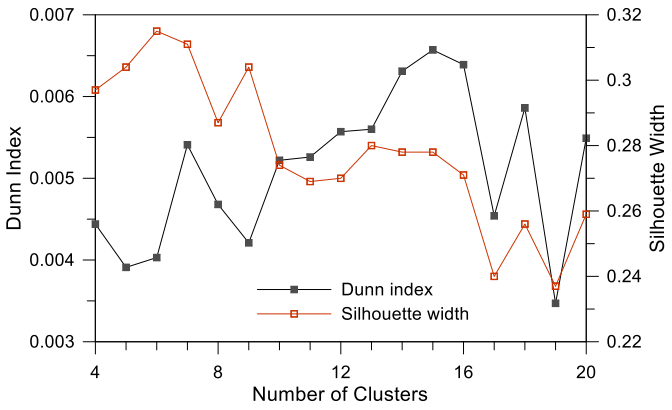

Fig. 2. Dunn index and silhouette width with different numbers of clusters.

3.3. Cluster identification

Since the Dunn index and silhouette width are high at seven clusters among 5 to 12 clusters as given in Table 1, the separations of clusters by increasing the number of clusters from 2 to 7 are shown in Fig. 3. For the characteristic values of the size distribution, the peak sizes and concentrations are presented in Fig. 3. We examined the variations in the peak size and number concentrations in Section S.1 in the supplement to determine the optimal number of clusters. The characteristics of clusters were distinguished based on the size distribution, diurnal variation in the occurrence, pollutant concentrations, and meteorological parameters. We chose seven as the optimal number of clusters, whose number size distribution, diurnal variations in the frequency of occurrence, and the selected pollutant concentrations and meteorological parameters are shown in Fig. 4 and Table 2, respectively.

Seven clusters can be grouped into four categories, BG, LocEm, TR, and NC by grouping 2 TRs into TR and 3 NCs into NC. We investigated the characteristics of four categories, including five subgroups (clusters), referring to Fig. 4 for the size distributions and diurnal variations in the frequency of occurrence, Fig. 5 for seasonal variations in the frequency of occurrence, and Fig. 6 for wind roses, along with Table 2 for selected pollutant concentrations and meteorological parameters. Table 3 presents the occurrence (%) and contributions (%) to the number concentrations by mode, which are defined by the fractions of the number concentration multiplied by the frequency of the occurrence.

3.3.1. BG (background)

The number concentration is lowest for all three modes. Pollutant concentrations are lower, but the ozone concentration is higher, than those for other clusters except for NC (Table 2). Despite no distinct diurnal variation in the frequency of occurrence, it increases slightly around 5:00 and 12:00 (Fig. 4(b)), probably because of transport of pollutants from distant pollution sources. The effects of BG became apparent in winter, when pollutant emissions and formation are suppressed, whereas the effects of BG were rarely observed in spring, when high concentrations of fugitive dust were frequent associated with high wind speeds and low RH (Choi et al., 2014; Ghim et al., 2015) (Fig. 5). Since the frequency of occurrence is high at 31%, following that of LocEm at 37% (Table 3), the wind rose is generally similar to that overall (Fig. 6). However, BG exhibits more frequent westerly winds along with east-northeasterly and easterly winds, although most emissions in the nearby area, including vehicle emissions, come from the valley entrance to the west-southwest, as seen in TR. This implies possible influences of pollution from a new town about 13 km west, and an expressway about 5 km east-northeast, of the study site.

3.3.2. LocEm (local emissions)

Many characteristics are similar to BG. However, pollutant concentrations are similar to those for TR, along with a low wind speed close to calm. In TR, the ozone concentration is low because of the titration of NO. Albeit larger than BG, the diurnal variation in the frequency of occurrence is also small and the frequency of occurrence is higher during

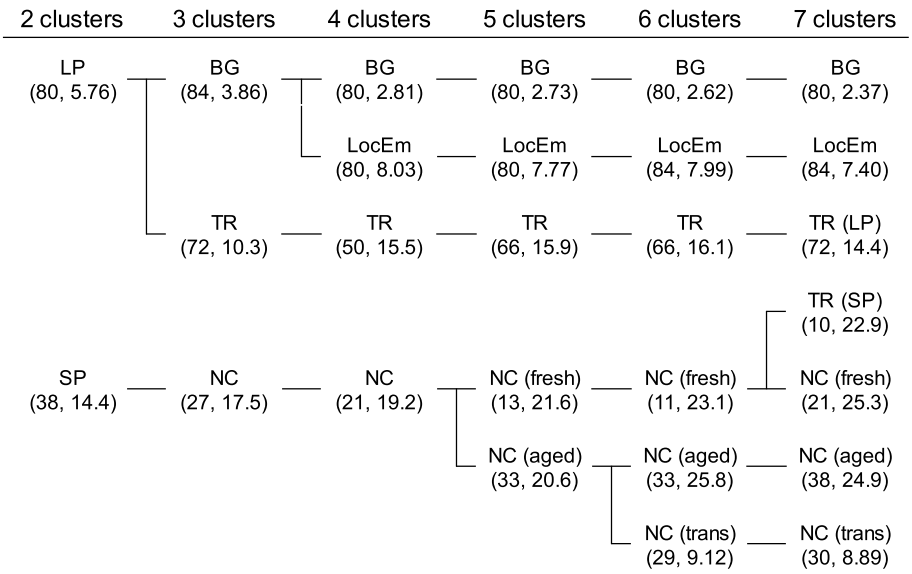

Fig. 3. Separation of clusters. Acronyms or abbreviations used for designating the clusters stand for: LP, larger particles; SP, smaller particles; BG, background; LocEm, local emissions; TR, traffic; NC, nucleation; NC (trans), NC (transported). The numbers in the parentheses denote peak size (nm) and peak number concentration (10^3 cm^{-3}).

Table 2
Selected pollutant concentrations and meteorological parameters for seven clusters. Boldface and underlined italics denote highest and lowest values, respectively.[a]

	Peak size (nm)	Peak time	Nucl (10^3 cm^{-3})	Aitken (10^3 cm^{-3})	Accum (10^3 cm^{-3})	SO_2 (ppb)	CO (ppm)	NO_2 (ppb)	O_3 (ppb)	PM_{10} ($\mu g/m^3$)	BC	SR (W/m^2)	Temp (°C)	RH (%)	WS (m/s)
BG	80	5:00, 12:00	*0.5*	*1.3*	*0.8*	5.33	0.66	29.1	24.3	52.0	1.20	221	11.3	**67.6**	1.34
LocEm	84	4:00	0.6	3.4	2.3	6.13	0.72	40.7	18.5	66.7	1.62	255	11.4	66.9	*0.56*
TR (LP)	72	9:00, 22:00	1.2	6.8	3.4	7.07	0.75	**45.0**	21.0	58.9	1.69	*220*	10.6	63.5	*0.56*
TR (SP)	10, 72	14:00	7.6	10.0	**4.9**	**9.24**	**0.79**	42.5	*17.5*	**67.3**	**1.84**	282	*4.6*	51.3	1.38
NC (fresh)	21	13:00	**8.4**	5.9	1.4	5.24	*0.51*	*20.1*	46.3	52.9	*0.88*	**564**	**18.9**	*35.1*	**2.73**
NC (aged)	38	16:00	3.1	**10.3**	1.8	*5.15*	0.52	27.2	**46.5**	*47.8*	0.99	359	15.5	43.7	1.86
NC (trans)	30	18:00	2.7	4.6	1.7	5.65	0.58	30.9	34.7	52.7	1.07	348	13.2	48.8	1.48

[a] Nucl, nucleation; Accum, accumulation; BC, black carbon; SR, solar radiation; Temp, air temperature; RH, relative humidity; WS, wind speed; NC (trans), NC (transported).

the night typified by the low mixing height at this time, while the emissions remain fairly constant throughout the day. Besides TR, we can consider biomass/open burning, biogenic emissions, and fugitive dust for local emissions at the study site. We excluded fuel combustion because of its high occurrence in winter. Fugitive dust is predominantly composed of coarse particles, but contains ultrafine particles, such as those caused by tire wear on the road (Kumar et al., 2013; Vu et al., 2015). However, at low wind speeds close to calm, the generation of fugitive dust should be low, and would hardly affect the study site that is not adjacent to the road. Although biogenic emissions can contribute to both primary emissions and secondary production, a high contribution in fall rather than spring and summer is implausible. Biomass/open burning differs widely from time to time and from region to region (Chen et al., 2017; Yin et al., 2019). However, if burning materials are crop residues, their burning will be frequent in fall. The measurement at the study site showed a high correlation of Cl^- with K^+, indicating the prevalence of biomass and open burning (Chow, 1995; Won et al., 2010; Li et al., 2012; Zauscher et al., 2013). In general, biomass/open burning, biogenic emissions, fugitive dust, and traffic belong to local emission sources. However, local emissions, excluding traffic that exhibits distinct diurnal patterns, remain fairly constant throughout the day. Biomass/open burning, biogenic emissions, and fugitive dust follow their own diurnal patterns, but these patterns offset each other once combined. Thus, no noticeable diurnal variation of LocEm was observed throughout the day as shown in Figs. S1 and S2.

Emissions may be small in winter because of low activity, but the cause of high emissions in summer when rainfall is frequent is unclear. The overall occurrence is highest at 37% (Table 3). Albeit low wind speeds associated with the overwhelming calm, the wind rose is generally similar to that overall.

3.3.3. TR (traffic emissions)

There are two types in TR, TR (LP) for larger particles and TR (SP) for smaller particles. Mean wind speed for TR (LP) is as low as LocEm with calm. Because of these low wind speeds, the effects of local emissions are manifest, and the occurrence peaks during the morning rush hour and is high in the evening hours, resulting from vehicle emissions from the neighborhood. On the other hand, despite being lower than that of NC, the wind speed for TR (SP) is relatively high, and the occurrence continues from the morning rush hour to the evening. Pollutant concentrations are generally high in TR, but are especially high for TR (SP), except for ozone. The number concentration of the Aitken mode is

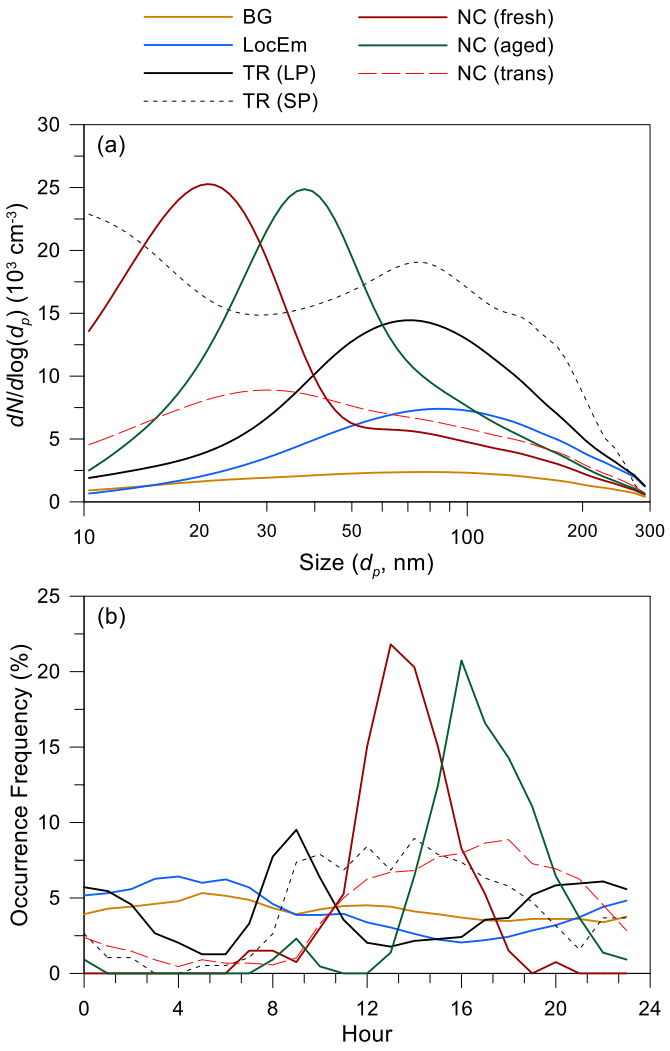

Fig. 4. (a) Number size distributions and (b) diurnal variations in the frequency of occurrence for seven clusters. *N* denotes the number concentration.

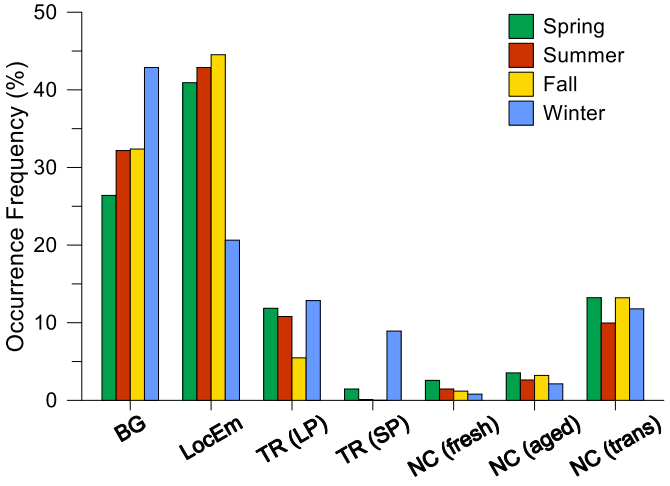

Fig. 5. Seasonal variations in the frequency of occurrence for seven clusters.

higher than for the other two modes. However, as mentioned earlier, because smaller and larger portions of the nucleation and accumulation modes, respectively, were not measured, only the relative values rather than the absolute values matter by mode. TR (SP) has the highest concentration in the nucleation mode except for NC (fresh), and has the primary peak at 10 nm, the lower limit. Although both TR (LP) and TR (SP) occur most frequently in winter, TR (SP) is unusual, because it occurs predominantly in winter. The wind roses in Fig. 6 show that both TR (LP) and TR (SP) are frequently affected by inflows from the west-southwest, the direction of the valley entrance. However, the influence from the west-southwest is dominant in TR (SP).

Particles emitted from vehicles generally display a bimodal distribution with peaks below 30 nm and above 50 nm (Myung and Park, 2012; Vu et al., 2015). The first mode consists of particles produced from high-temperature exhaust by condensation or nucleation immediately after being released into the atmosphere, whereas the second mode consists of mostly carbonaceous materials in the form of soot. In Fig. 4 (a), the second-mode peak for TR (SP) is similar to that for TR (LP). In fact, it is known that the first mode shows a large variation with distance from the road. In Los Angeles, the first mode diminished with distance and disappeared (Zhu et al., 2002a, b; Zhang et al., 2004), whereas in London, the peak size of the first mode shrank with distance, as semi-volatile substances volatilized at ~8 °C in the fall (Dall'Osto et al., 2011a). Thus, we can presume that the primary peak for TR (SP) at 10 nm resulted from the reduction of particles in the first mode by volatilization, while being rapidly transported from the road in winter. We can also presume that the first mode diminished and disappeared in warm seasons, causing TR (LP). Because of the direct effects of vehicle emissions for TR (SP), most pollutant concentrations are highest in Table 2, and the influence from the west-southwest toward the valley entrance, through which vehicle emissions from the national road inflow, is dominant in Fig. 6. Frequent occurrence of TR (SP) during the daytime in Fig. 4(b) is attributable to favorable meteorological conditions for rapid transport and volatilization, such as higher wind speeds and solar radiation, respectively.

Despite the smallest peak size at 10 nm for TR (SP), the contribution to the nucleation mode is lower than those for NC (trans) and LocEm, because of a low frequency of occurrence only at 2.7% in Table 3. On the other hand, the number concentration in the Aitken mode is not very high for TR (LP) (Table 2), but its contribution to the Aitken mode is second to LocEm along with that to the accumulation mode, because the frequency of occurrence is 4th out of 7 clusters in Table 3.

3.3.4. NC (nucleation)

NC is divided into NC (fresh) denoting locally nucleated, NC (aged) denoting that locally nucleated particles are aged, and NC (trans) denoting that particles nucleated from a distance are transported. NC (fresh) has the highest concentration in the nucleation mode, and the lowest concentrations of CO, NO_2 and BC mainly emitted from vehicles (Vehkamäki et al., 2004; Hamed et al., 2007; Lee et al., under review). It also has the highest solar radiation, temperature, and wind speed, and the lowest RH, which are all favorable for NPF (Vehkamäki et al., 2004; Hamed et al., 2007; Jeong et al., 2010; Kerminen et al., 2018). NC (aged) has the highest Aitken-mode concentration. Ozone concentration is highest and PM_{10} is lowest, so low-volatile substances are actively produced via photochemical reactions, while the condensation sink of these substances onto existing particles is unavailable. These conditions are conducive to subsequent growth after the formation of particles (Kerminen et al., 2018, and references therein). However, SO_2 concentrations are generally low for all NCs, which is the main precursor of sulfate (a key element of NPF), perhaps because the concentrations of primary pollutants including PM_{10} were high at high SO_2 concentrations, which is disadvantageous for NPF.

In Fig. 4(a) and (b), the peak size of 21 nm and peak time of 13:00 for NC (fresh) are the smallest and earliest, respectively, among NCs. For NC (aged), the peak size increases to 38 nm, and the peak time delays to 16:00, because of the growth of nucleated particles. Many features for NC (trans) shown in Table 2 and Fig. 4(a) are similar to those for BG and LocEm rather than to the other two NCs. The occurrence of NC (trans) for a long time from the beginning of NC (fresh) to the end of NC (aged)

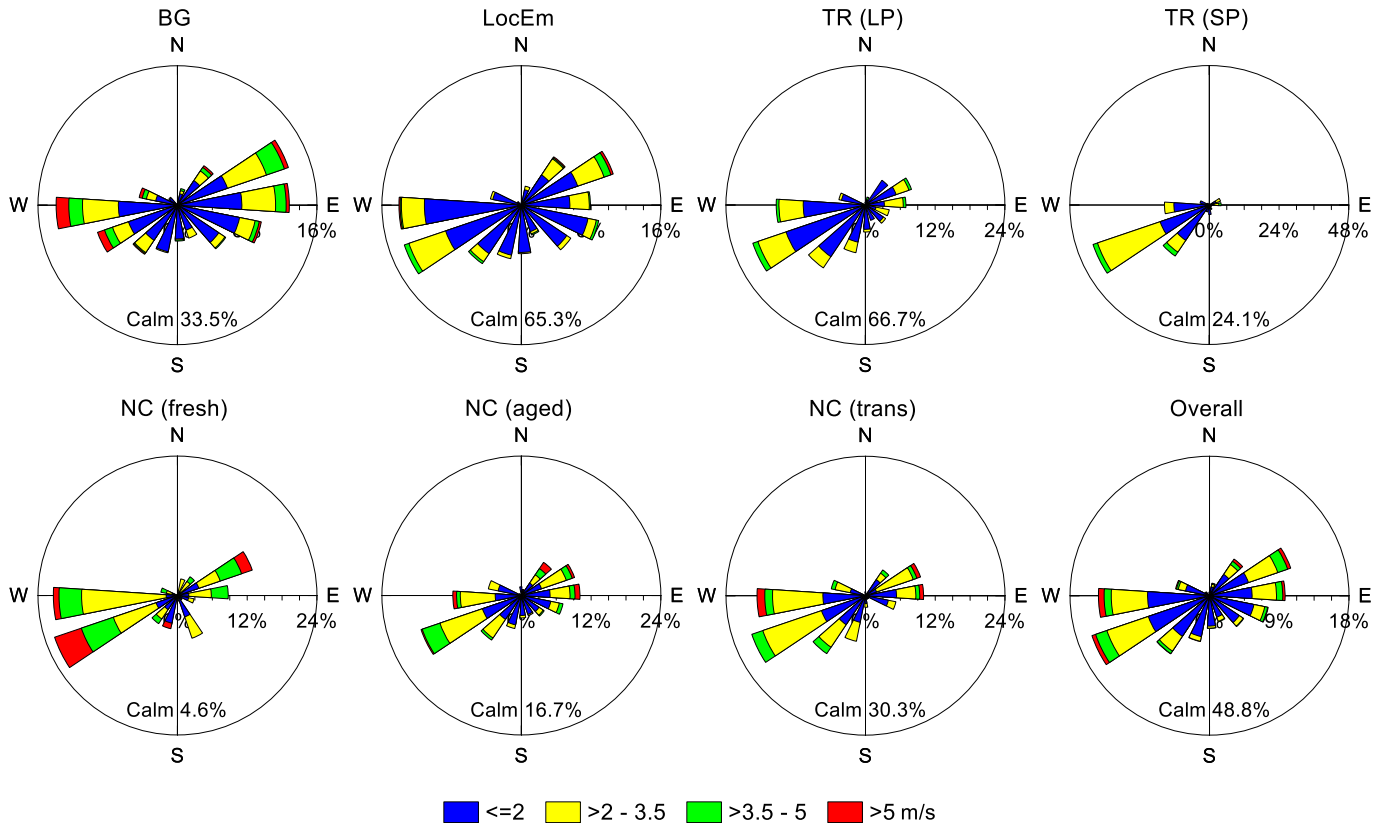

Fig. 6. Wind roses for seven clusters. Note that the maximum values of the radius ranges from 16% to 48%. Calm denotes a wind speed of less than 0.5 m/s.

Table 3
Frequency of occurrence and contributions[a] to the number concentrations by mode for seven clusters.

	Frequency of occurrence	Contribution			
		Nucleation	Aitken	Accumulation	Total
BG	31.4%	12.7%	11.2%	12.7%	11.9%
LocEm	37.3%	16.8%	34.3%	44.7%	33.8%
TR sum	13.9%	26.1%	27.7%	26.8%	27.1%
NC sum	17.4%	44.4%	26.9%	15.8%	27.2%
TR (LP)	11.2%	10.5%	20.4%	19.8%	18.3%
TR (SP)	2.7%	15.6%	7.3%	7.0%	8.8%
NC (fresh)	1.9%	12.0%	3.0%	1.4%	4.3%
NC (aged)	3.1%	7.2%	8.5%	3.0%	6.8%
NC (trans)	12.5%	25.2%	15.4%	11.5%	16.2%

[a] Defined by the fraction of the number concentration multiplied by the frequency of the occurrence.

could result from the NPF occurrences over a wide area. The seasonal variations in how often NCs occur (Fig. 5), which is high in spring and low in summer or fall, are generally comparable to those reported for Korea (Lee et al., 2008; Kim et al., 2013; Park et al., 2015). The wind rose for NC (fresh) exhibits a strong influence from the west-southwest and west, albeit not as extreme as that for TR (SP) (Fig. 6). Despite lower frequency than for west-southwesterly and westerly, high wind speeds of the east-northeasterly may indicate the effects of biogenic emissions from the eastern mountainous area associated with the valley-mountain breeze.

3.4. Contribution to the number concentrations by mode

As already mentioned, the absolute values of the number concentrations shown in Table 2 do not have much significance because we excluded the smaller and larger parts of the nucleation and accumulation modes, respectively. Therefore, we calculated the contribution of each cluster to the number concentration by multiplying the number concentration by the frequency of the occurrence in Table 3. Looking at the size distributions in Fig. 4, the number concentration for TR (SP) would be much higher and that for NC (fresh) would increase if we measured the size distribution below 10 nm. However, the increases of the contributions for both TR (SP) and NC (fresh) are limited, because they did not occur frequently. In the accumulation mode, we excluded the size more than ~300 nm, but Fig. 4 reveals that the contributions from such a size to the number concentrations are small for all clusters.

For the total number concentration, the contribution of LocEm is largest because it occurs the most frequently, and its contributions to the Aitken and accumulation modes are also large at 34% and 45%, respectively. For the nucleation mode, the contribution of the NC sum is largest at 44%, and that of NC (trans) is largest at 25% because it occurs the most frequently among NCs. That the contribution of the TR sum is smaller than that of the NC sum could be ascribed to the location of the study site, which is more than 1 km away from the main road.

4. Summary and conclusions

We investigated the number size distribution patterns at a rural site downwind of Seoul, Korea, based on SMPS measurements in the range of 10.3–290.8 nm for the period February 2015 through June 2016, using *k*-means clustering. Seven clusters categorized as background (BG), local emissions (LocEm), traffic emissions (TR), and nucleation (NC) were identified. TR was further divided into TR (LP) for larger particles and TR (SP) for smaller particles, and NC was divided into NC (fresh) denoting locally nucleated, NC (aged) denoting locally nucleated but aged, and NC (trans) denoting nucleated from a distance and transported. The following summarize key findings from this study:

(1) BG had the lowest number concentrations for all modes, and the concentrations of primary pollutants were also lower than those for other clusters except for NCs. For LocEm, pollutant concentrations were as high as TR because of low wind conditions near calm, and frequent occurrence at dawn with low mixing heights implied that diurnal variations in emissions were not large. Biomass and open burning were the most likely sources for LocEm.
(2) TR (LP) was typical of vehicle emissions, occurring frequently during the morning rush hours and the evening hours. Particles emitted from vehicles generally show a bimodal distribution, with peaks below 30 nm and above 50 nm. Because the study site is more than 1 km away from the main road, the first mode (mostly in the nucleation mode) disappeared by volatilization and only the second mode was measured in TR (LP). On the other hand, in TR (SP), the particle size of the first mode was reduced by the volatilization of semi-volatile substances, while being rapidly transported from the road in winter. Most of the primary pollutant concentrations were highest because of the direct effects of vehicle emissions.
(3) NC (fresh) exhibited the highest concentration in the nucleation mode. The peak size of 21 nm and the peak time of 13:00 were the smallest and earliest, respectively, among NCs. Along with the highest solar radiation, temperature, wind speed, and lowest RH, the lowest concentrations of pollutants emitted from vehicles were favorable for NPF. NC (aged) was characterized by the highest ozone concentration that could be linked to active production of low-volatile substances, and the lowest PM_{10} concentration that could be linked to the unavailability of a condensation sink by pre-existing particles. NC (trans) had many characteristics similar to BG and LocEm, indicating NPF over a wider area.
(4) LocEm contributed the most, at 34%, to the total number concentration, because it occurred the most frequently. The contribution to the nucleation mode was highest at 44% for NC compared to 26% for TR, because of the distance between the study site and the main road.

CRediT author statement

Y. Lee: Formal analysis, Data curation, Writing – Original Draft; Y, Choi: Data curation; J. Park: Conceptualization, Methodology, Writing – Original Draft; H. An, Y. Lee: Investigation, Resources; Y. S. Ghim: Validation, Writing – Review and Editing, Supervision, Project administration.

Declaration of competing interest

The authors declare that they have no known competing financial interests or personal relationships that could have appeared to influence the work reported in this paper.

Acknowledgements

This study was supported by a National Research Foundation of Korea (NRF) grant funded by the Korean government (MSIT) (NRF-2019R1F1A1058127) and the Hankuk University of Foreign Studies Research Fund. We thank the National Institute of Environmental Research for providing pollutant concentrations through https://www.airkorea.or.kr/web/last_amb_hour_data?pMENU_NO=123 (in Korean), and the Korea Meteorological Administration for providing meteorological data through http://www.kma.go.kr/weather/observation/currentweather.jsp (in Korean).

Appendix A. Supplementary data

Supplementary data to this article can be found online at https://doi.org/10.1016/j.apr.2021.101086.

References

Agudelo-Castañeda, D.M., Teixeira, E.C., Braga, M., Rolim, S.B.A., Silva, L.F.O., Beddows, D.C.S., Harrison, R.M., Querol, X., 2019. Cluster analysis of urban ultrafine particles size distributions. Atmos. Pollut. Res. 10 (1), 45–52. https://doi.org/10.1016/j.apr.2018.06.006.

Beddows, D.C.S., Dall'Osto, M., Harrison, R.M., 2009. Cluster analysis of rural, urban, and curbside atmospheric particle size data. Environ. Sci. Technol. 43 (13), 4694–4700. https://doi.org/10.1021/es803121t.

Brilke, S., Fölker, N., Müller, T., Kandler, K., Gong, X., Peischl, J., Weinzierl, B., Winkler, P.M., 2020. New particle formation and sub-10 nm size distribution measurements during the A-LIFE field experiment in Paphos, Cyprus. Atmos. Chem. Phys. 20 (9), 5645–5656. https://doi.org/10.5194/acp-20-5645-2020.

Brines, M., Dall'Osto, M., Beddows, D.C.S., Harrison, R.M., Gómez-Moreno, F., Núñez, L., Artíñano, B., Costabile, F., Gobbi, G.P., Salimi, F., Morawska, L., Sioutas, C., Querol, X., 2015. Traffic and nucleation events as main sources of ultrafine particles in high-insolation developed world cities. Atmos. Chem. Phys. 15 (10), 5929–5945. https://doi.org/10.5194/acp-15-5929-2015.

Brines, M., Dall'Osto, M., Beddows, D.C.S., Harrison, R.M., Querol, X., 2014. Simplifying aerosol size distributions modes simultaneously detected at four monitoring sites during SAPUSS. Atmos. Chem. Phys. 14 (6), 2973–2986. https://doi.org/10.5194/acp-14-2973-2014.

Brock, G., Pihur, V., Datta, Susmita, Datta, Somnath, 2008. clValid, an R package for cluster validation. J. Stat. Software 25 (4). https://doi.org/10.18637/jss.v025.i04.

Chen, J., Li, C., Ristovski, Z., Milic, A., Gu, Y., Islam, M.S., Wang, S., Hao, J., Zhang, H., He, C., Guo, H., Fu, H., Miljevic, B., Morawska, L., Thai, P., Lam, Y.F., Pereira, G., Ding, A., Huang, X., Dumka, U.C., 2017. A review of biomass burning: emissions and impacts on air quality, health and climate in China. Sci. Total Environ. 579, 1000–1034. https://doi.org/10.1016/j.scitotenv.2016.11.025.

Choi, S.-H., Ghim, Y.S., Chang, Y.-S., Jung, K., 2014. Behavior of particulate matter during high concentration episodes in Seoul. Environ. Sci. Pollut. Res. 21, 5972–5982. https://doi.org/10.1007/s11356-014-2555-y.

Chow, J.C., 1995. Measurement methods to determine compliance with ambient air quality standards for suspended particles. J. Air Waste Manag. Assoc. 45 (5), 320–382.

Dall'Osto, M., Querol, X., Alastuey, A., O'Dowd, C., Harrison, R.M., Wenger, J., Gómez-Moreno, F.J., 2013. On the spatial distribution and evolution of ultrafine particles in Barcelona. Atmos. Chem. Phys. 13 (2), 741–759. https://doi.org/10.5194/acp-13-741-2013.

DallÓsto, M., Beddows, D.C.S., Pey, J., Rodriguez, S., Alastuey, A., Harrison, R.M., Querol, X., 2012. Urban aerosol size distributions over the Mediterranean city of Barcelona, NE Spain. Atmos. Chem. Phys. 12 (22), 10693–10707. https://doi.org/10.5194/acp-12-10693-2012.

DallÓsto, M., Thorpe, A., Beddows, D.C.S., Harrison, R.M., Barlow, J.F., Dunbar, T., Williams, P.I., Coe, H., 2011a. Remarkable dynamics of nanoparticles in the urban atmosphere. Atmos. Chem. Phys. 11 (13), 6623–6637. https://doi.org/10.5194/acp-11-6623-2011.

Dall'Osto, M., Monahan, C., Greaney, R., Beddows, D.C.S., Harrison, R.M., Ceburnis, D., O'Dowd, C.D., 2011b. A statistical analysis of North East Atlantic (submicron) aerosol size distributions. Atmos. Chem. Phys. 11, 12567–12578. https://doi.org/10.5194/acp-11-12567-2011.

Forster, P., Ramaswamy, V., Artaxo, P., Berntsen, T., Betts, R., Fahey, D.W., Haywood, J., Lean, J., Lowe, D.C., Myhre, G., 2007. Changes in atmospheric constituents and in radiative forcing. In: Chapter 2. Climate Change 2007. The Physical Science Basis. Contribution of Working Group I to the Fourth Assessment Report of the Intergovernmental Panel on Climate Change. Cambridge University Press, Cambridge, England and New York, NY.

Fujita, E.M., Stockwell, W.R., Campbell, D.E., Keislar, R.E., Lawson, D.R., 2003. Evolution of the magnitude and spatial extent of the weekend ozone effect in California's south coast air basin, 1981–2000. J. Air Waste Manag. Assoc. 53 (7), 802–815. https://doi.org/10.1080/10473289.2003.10466225.

Ghim, Y.S., Chang, Y.-S., Jung, K., 2015. Temporal and spatial variations in fine and coarse particles in Seoul, Korea. Aerosol Air Qual. Res. 15, 842–852. https://doi.org/10.4209/aaqr.2013.12.0362.

Ghim, Y.S., Chang, Y.-S., 2000. Characteristics of ground-level ozone distributions in Korea for the period of 1990-1995. J. Geophys. Res. 105 (D7), 8877–8890. https://doi.org/10.1029/1999JD901179.

Hamed, A., Joutsensaari, J., Mikkonen, S., Sogacheva, L., Maso, M.D., Kulmala, M., Cavalli, F., Fuzzi, S., Facchini, M.C., Decesari, S., Mircea, M., Lehtinen, K.E.J., Laaksonen, A., 2007. Nucleation and growth of new particles in Po Valley, Italy. Atmos. Chem. Phys. 7, 355–376. https://doi.org/10.5194/acp-7-355-2007.

HEI Review Panel on Ultrafine Particles, 2013. Understanding the Health Effects of Ambient Ultrafine Particles. HEI Perspectives, vol. 3. Health Effects Institute, Boston, Massachusetts.

Jeong, C.-H., Evans, G.J., McGuire, M.L., Chang, R.Y.-W., Abbatt, J.P.D., Zeromskiene, K., Mozurkewich, M., Li, S.-M., Leaitch, W.R., 2010. Particle formation and growth at five rural and urban sites. Atmos. Chem. Phys. 10, 7979–7995. https://doi.org/10.5194/acp-10-7979-2010.

Kanaya, Y., Taketani, F., Komazaki, Y., Liu, X., Kondo, Y., Sahu, L.K., Irie, H., Takashima, H., 2013. Comparison of black carbon mass concentrations observed by multi-angle Absorption photometer (MAAP) and continuous soot-monitoring system (COSMOS) on Fukue Island and in Tokyo, Japan. Aerosol Sci. Technol. 47 (1), 1–10. https://doi.org/10.1080/02786826.2012.716551.

Kerminen, V.-M., Chen, X., Vakkari, V., Petäjä, T., Kulmala, M., Bianchi, F., 2018. Atmospheric new particle formation and growth: review of field observations. Environ. Res. Lett. 13, 103003. https://doi.org/10.1088/1748-9326/aadf3c.

Kim, Y., Yoon, S.-C., Kim, S.-W., Kim, K.-Y., Lim, H.-C., Ryu, J., 2013. Observation of new particle formation and growth events in Asian continental outflow. Atmos. Environ. 64, 160–168. https://doi.org/10.1016/j.atmosenv.2012.09.057.

Kontkanen, J., Lehtipalo, K., Ahonen, L., Kangasluoma, J., Manninen, H.E., Hakala, J., Rose, C., Sellegri, K., Xiao, S., Wang, L., Qi, X., Nie, W., Ding, A., Yu, H., Lee, S., Kerminen, V.-M., Petäjä, T., Kulmala, M., 2017. Measurements of sub-3 nm particles using a particle size magnifier in different environments: from clean mountain top to polluted megacities. Atmos. Chem. Phys. 17, 2163–2187. https://doi.org/10.5194/acp-17-2163-2017.

Kulmala, M., Petäjä, T., Ehn, M., Thornton, J., Sipilä, M., Worsnop, D.R., Kerminen, V.-M., 2014. Chemistry of atmospheric nucleation: on the recent advances on precursor characterization and atmospheric cluster composition in connection with atmospheric new particle formation. Annu. Rev. Phys. Chem. 65, 21–37.

Kumala, M., Asmi, A., Lappalainen, H.K., Baltensperger, U., Brenguier, J.L., Facchini, M.C., Hansson, H.C., 2011. General overview: general overview European Integrated project on Aerosol Cloud Climate and Air Quality interactions (EUCAARI)—integrating aerosol research from nano to global scales. Atmos. Chem. Phys. 11, 13061–13143.

Kumar, P., Pirjola, L., Ketzel, M., Harrison, R.M., 2013. Nanoparticle emissions from 11 non-vehicle exhaust sources – a review. Atmos. Environ. 67, 252–277. https://doi.org/10.1016/j.atmosenv.2012.11.011.

Lee, S.-H., Gordon, H., Yu, H., Lehtipalo, K., Haley, R., Li, Y., Zhang, R., 2019. New particle formation in the atmosphere: from molecular clusters to global climate. J. Geophys. Res. Atmos. 124, 7098–7146. https://doi.org/10.1029/2018JD029356.

Lee, Y.-G., Lee, H.-W., Kim, M.-S., Choi, C.Y., Kim, J., 2008. Characteristics of particle formation events in the coastal region of Korea in 2005. Atmos. Environ. 42, 3729–3739. https://doi.org/10.1016/j.atmosenv.2007.12.064.

Lee, Y., Park, J., Kim, P., Ghim, Y. S. New Particle Formation and Diurnal Variations in Number Concentrations at a Rural Site Downwind of Seoul, Korea. (submitted for publication).

Li, G., Lei, W., Bei, N., Molina, L.T., 2012. Contribution of garbage burning to chloride and $PM_{2.5}$ in Mexico City. Atmos. Chem. Phys. 12, 8751–8761. https://doi.org/10.5194/acp-12-8751-2012.

Myung, C.L., Park, S., 2012. Exhaust nanoparticle emissions from internal combustion engines: a review. Int. J. Automot. Technol. 13 (1), 9–22. https://doi.org/10.1007/s12239-012-0002-y.

NARSTO, 2004. In: McMurry, P.H., Shepherd, M.F., Vickery, J.S. (Eds.), Particulate Matter Science for Policy Makers: A NARSTO Assessment. Cambridge University Press, Cambridge, England.

Paasonen, P., Kupiainen, K., Klimont, Z., Visschedijk, A., Denier van der Gon, H.A.C., Amann, M., 2016. Continental anthropogenic primary particle number emissions. Atmos. Chem. Phys. 16, 6823–6840. https://doi.org/10.5194/acp-16-6823-2016.

Park, M., Yum, S.S., Kim, J.H., 2015. Characteristics of submicron aerosol number size distribution and new particle formation events measured in Seoul, Korea, during 2004–2012. Asia-Pacific J. Atmos. Sci. 51, 1–10. https://doi.org/10.1007/s13143-014-0055-0.

Qi, X.M., Ding, A.J., Nie, W., Petäjä, T., Kerminen, V.-M., Herrmann, E., Xie, Y.N., Zheng, L.F., Manninen, H., Aalto, P., Sun, J.N., Xu, Z.N., Chi, X.G., Huang, X., Boy, M., Virkkula, A., Yang, X.-Q., Fu, C.B., Kulmala, M., 2015. Aerosol size distribution and new particle formation in the western Yangtze River Delta of China: 2 years of measurements at the SORPES station. Atmos. Chem. Phys. 15, 12445–12464. https://doi.org/10.5194/acp-15-12445-2015.

Ripamonti, G., Järvi, L., Mølgaard, B., Hussein, T., Nordbo, A., Hämeri, K., 2013. The effect of local sources on aerosol particle number size distribution, concentrations and fluxes in Helsinki, Finland. Tellus Ser. B Chem. Phys. Meteorol. 65 (1), 19786 https://doi.org/10.3402/tellusb.v65i0.19786.

Sabaliauskas, K., Jeong, C.-H., Yao, X., Jun, Y.-S., Evans, G., 2013. Cluster analysis of roadside ultrafine particle size distributions. Atmos. Environ. 70, 64–74. https://doi.org/10.1016/j.atmosenv.2012.12.025.

Salimi, F., Ristovski, Z., Mazaheri, M., Laiman, R., Crilley, L.R., He, C., Clifford, S., Morawska, L., 2014. Assessment and application of clustering techniques to atmospheric particle number size distribution for the purpose of source apportionment. Atmos. Chem. Phys. 14 (21), 11883–11892. https://doi.org/10.5194/acp-14-11883-2014.

Schraufnagel, D.E., 2020. The health effects of ultrafine particles. Exp. Mol. Med. 52, 311–317. https://doi.org/10.1038/s12276-020-0403-3.

Seinfeld, J.H., Pandis, S.N., 2006. Atmospheric Chemistry and Physics: from Air Pollution to Climate Change. Wiley.

Vehkamaki, H., Maso, M.D., Hussein, T., Flanagan, R., Hyvarinen, A., Lauros, J., Merikanto, J., Monkkonen, P., Pihlatie, M., Salminen, K., Sogacheva, L., Thum, T., Ruuskanen, T.M., Keronen, P., Aalto, P.P., Hari, P., Lehtinen, K.E.J., Rannik, U., Kulmala, M., 2004. Atmospheric particle formation events at Värriö measurement station in Finnish Lapland 1998–2002. Atmos. Chem. Phys. 4, 2015–2023.

Vu, T.V., Delgado-Saborit, J.M., Harrison, R.M., 2015. Review: particle number size distributions from seven major sources and implications for source apportionment studies. Atmos. Environ. 122, 114–132. https://doi.org/10.1016/j.atmosenv.2015.09.027.

Wang, Z.B., Hu, M., Wu, Z.J., Yue, D.L., He, L.Y., Huang, X.F., Liu, X.G., Wiedensohler, A., 2013. Long-term measurements of particle number size distributions and the relationships with air mass history and source apportionment in the summer of Beijing. Atmos. Chem. Phys. 13, 10159–10170. https://doi.org/10.5194/acp-13-10159-2013.

Wegner, T., Hussein, T., Hämeri, K., Vesala, T., Kulmala, M., Weber, S., 2012. Properties of aerosol signature size distributions in the urban environment as derived by cluster analysis. Atmos. Environ. 61, 350–360. https://doi.org/10.1016/j.atmosenv.2012.07.048.

Won, S.-R., Choi, Y.-J., Kim, A., Choi, S.-H., Ghim, Y.-S., 2010. Ion concentrations of particulate matter in Yongin in spring and fall. Journal of Korean Society for Atmos. Environ. 26 (3), 265–275 (in Korean with English abstract).

World Health Organization, 2013. Review of Evidence on Health Aspects of Air Pollution – REVIHAAP Project Technical Report. WHO Regional Office for Europe, Copenhagen, Denmark, p. 309.

World Health Organization, 2003. Health Aspects of Air Pollution with Particulate Matter, Ozone and Nitrogen Dioxide. Report on a WHO working group. WHO Regional Office for Europe, Copenhagen, Denmark.

Yin, L., Du, P., Zhang, M., Liu, M., Xu, T., Song, Y., 2019. Estimation of emissions from biomass burning in China (2003–2017) based on MODIS fire radiative energy data. Biogeosciences 16 (7), 1629–1640. https://doi.org/10.5194/bg-16-1629-2019.

Zauscher, M.D., Wang, Y., Moore, M.J.K., Gaston, C.J., Prather, K.A., 2013. Air quality impact and physicochemical aging of biomass burning aerosols during the 2007 san Diego wildfires. Environ. Sci. Technol. 47 (14), 7633–7643. https://doi.org/10.1021/es4004137.

Zhang, K.M., Wexler, A.S., Zhu, Y.F., Hinds, W.C., Sioutas, C., 2004. Evolution of particle number distribution near roadways. Part II: the 'Road-to-Ambient' process. Atmos. Environ. 38, 6655–6665. https://doi.org/10.1016/j.atmosenv.2004.06.044.

Zhu, Y., Hinds, W.C., Kim, S., Sioutas, C., 2002a. Concentration and size distribution of ultrafine particles near a major highway. J. Air Waste Manag. Assoc. 52 (9), 1032–1042.

Zhu, Y., Hinds, W.C., Kim, S., Shen, S., Sioutas, C., 2002b. Study of ultrafine particles near a major highway with heavy-duty diesel traffic. Atmos. Environ. 36, 4323–4335. https://doi.org/10.1016/S1352-2310(02)00354-0.